[3] E. C. Burdette, F. L. Cain, and J. Seals, "In vivo probe measurement technique for determining properties at VHF through microwave frequencies," *IEEE Trans. Microwave Theory Tech.*, vol. MTT-28, p. 414, 1980.
[4] J. B. Hasted, *Aqueous Dielectrics*. London, England: Chapman and Hall, 1973, ch. 8, pp. 204–233.
[5] E. H. Grant, R. J. Sheppard, and G. P. South, *Dielectric Behavior of Biological Molecules in Solution*. London, England: Oxford Univ. Press, 1978.
[6] J. Behari, H. Kumar, and R. Aruna, "Effect of ultraviolet light on dielectric properties of bone at microwave frequencies," to be published in *Annals Biomed. Eng.*
[7] T. W. Dakins and C. N. Works, "Microwave dielectric measurements," *J. Appl. Phys.*, vol. 18, p. 781, 1947.
[8] N. E. Hill, W. E. Vaughan, A. H. Price, and M. H. Davies, *Dielectric Properties and Molecular Behavior*. London, England: Von Nostrand Reinhold, 1969.
[9] L. H. K. Van Beek, "Dielectric behavior of heterogeneous systems," in *Progress in Dielectrics*, J. B. Birks, Ed., vol. 7, pp. 69–114, 1967.
[10] H. A. Bethe and J. Schwinger, "Perturbation theory of resonant cavities," NDRC Rep. L4-117, Radiation Laboratory, MIT, 1943.
[11] D. C. Dube and R. Parshad, "Study of Bottcher's formula for dielectric correlation between powder and bulk," *J. Phys. D.*, vol. 3, p. 677, 1970.
[12] D. C. Dube, "Study of Landau-Lifshitz-Looyenga's formula for dielectric correlation between powder and bulk," *J. Phys. D.*, vol. 3, p. 1648, 1970.
[13] C. J. F. Bottcher and P. Bordwijk, *Theory of Electric Polarization*, vol. II. Amsterdam, The Netherlands: Elsevier, 1978, pp. 206–207.
[14] D. Crowfoot, "X-ray crystallography and sterol structure," *Vitamin and Hormones*, vol. 2, p. 409, 1944.
[15] *CRC Handbook of Chemistry and Physics*. Ohio: CRC Press, 58th ed., 1977–1978, pp. C-246, C-444.
[16] G. P. Johari, J. Crossley, and C. P. Smyth, "The relaxation process of several long chain aliphatic molecules in n-heptane solutions," *J. Amer. Chem. Soc.*, vol. 91, p. 5197, 1969.
[17] L. K. Ngai, A. K. Jonscher, and C. T. White, "On the origin of the universal dielectric response in condensed matter," *Nature*, vol. 277, pp. 185–189, 1979.
[18] J. R. Rabinwitz, "Possible mechanisms for the biomolecular absorption of microwave radiation with functional implications," *IEEE Trans. Microwave Theory Tech.*, vol. MTT-21, pp. 850–851, 1973.

R. Aruna received the M.Sc. degree in physics from the University of Delhi, Delhi, India. She is currently working towards the Ph.D. degree at Jawaharlal Nehru University, New Delhi, as a C.S.I.R. Research Fellow.

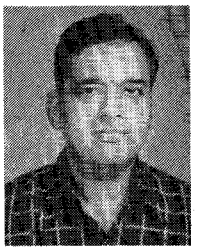

J. Behari received the Ph.D. degree in physics from the Indian Institute of Technology, Delhi, in 1971.

Thereafter, he worked in the same Institute in the Biomedical Engineering Centre in the field of reproductive engineering. In 1976, he joined the Jawaharlal Nehru University as an Assistant Professor. His current research interests include: bioelectric bone behavior, interaction of ultrasound, low-frequency electromagnetic waves, and microwaves with biological systems.

Analysis of Miniature Electric Field Probes with Resistive Transmission Lines

GLENN S. SMITH, SENIOR MEMBER, IEEE

Abstract—**The miniature dipole probe is a useful tool for measuring the electric field at high radio and microwave frequencies. A common design for the probe consists of an electrically short dipole antenna with a diode across its terminals; a resistive, parallel-wire transmission line transmits the detected signal from the diode to the monitoring instrumentation. The high resistance per unit length of the transmission line reduces the direct reception of the incident field by the line and also reduces the scattering of the incident field by the line. In addition, the resistive transmission line serves as a low-pass filter in the detection process. In this paper, the effect of the resistive transmission line on the operation of the miniature field probe is analyzed. Specifically, the reception of the incident signal by the transmission line is compared with that of the dipole. The scattering of the incident signal by the transmission line is studied by means of the scattering cross section, and the limitation imposed on the measurement of amplitude-modulated signals by the low-pass filtering by the resistive line is examined. The results of the theoretical analyses are presented as simple formulas which are useful in the design and optimization of the probe. The theoretical results are shown to be in good agreement with measurements.**

Manuscript received April 6, 1981; revised June 29, 1981. This work was supported by the National Science Foundation under Grant ENG78-18273 through a subgrant to the Georgia Institute of Technology from the University of Virginia, Charlottesville.

The author is with the School of Electrical Engineering, Georgia Institute of Technology, Atlanta, GA 30332.

I. INTRODUCTION

IN MANY practical applications of electromagnetism at high radio and microwave frequencies, an accurate measurement of the electric field in free space or in a material medium is required. Examples are the calibration of electromagnetic shielded rooms and anechoic chambers, the measurement of the near field of transmitting antennas,

0018-9480/81/1100-1213$00.75 ©1981 IEEE

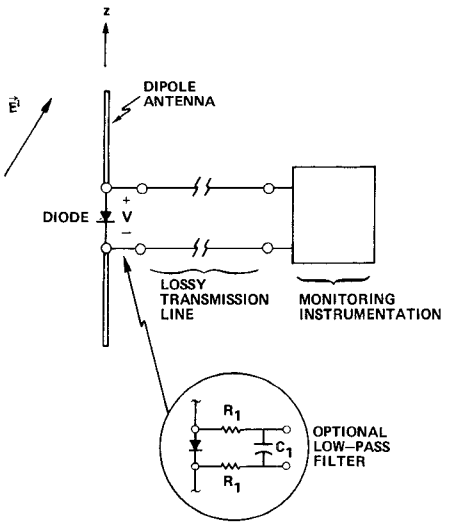

Fig. 1. Dipole receiving probe.

and the sensing of fields in and around transmission lines and waveguides. In addition, the recent interest in the biological effects of nonionizing electromagnetic radiation has created a need to measure the electric field in free space for hazard assessment of emissions from devices, such as microwave ovens, and in biological tissue or simulated tissue to provide dosimetry for controlled bioelectromagnetic experiments.

The electrically short receiving dipole antenna is ideally suited to this measurement, because the voltage produced at its terminals is proportional to the component of the incident electric field $\boldsymbol{E}^i$ that is parallel to its axis. With reference to Fig. 1, the terminal voltage V is

$$V = K_e \boldsymbol{E}^i \cdot \hat{z} \tag{1}$$

where K_e is the constant of proportionality. For a practical probe, a connection that does not perturb the measurement of the electric field must be made between the dipole and the instrumentation that monitors the voltage V. A number of dipole probes have been constructed using the basic connection shown schematically in Fig. 1. The operation of this probe is fairly simple. For an amplitude-modulated incident field, the dipole produces an amplitude-modulated oscillating voltage across the diode at its terminals. When the diode is operating in its square-law region, a current proportional to the square of the modulating signal is also developed at the diode. For example, a continuous wave field produces a direct current at the diode. This current is passed through the low-pass filter formed by the lossy transmission line to the monitoring instrumentation. Thus a signal proportional to the square of the amplitude modulation on the incident field is measured. The high resistance per unit length of the lossy transmission line reduces the signal received directly by the line and transmitted to the diode; it also reduces the scattering of the incident field by the transmission line. In some probe designs, an additional discrete-element low-pass filter is placed between the diode and the transmission line as the insert in Fig. 1 shows.

The transmission lines for early versions of this probe were constructed from very thin metallic wire with a typical resistance per unit length being 0.1–1 kΩ/m [1], [2]. Later versions used a "semiconducting" line developed by the U.S. National Bureau of Standards (NBS) [3]. This line is formed from polytetraflouroethylene (Teflon) impregnated with finely divided carbon black; the resistance per unit length for a 0.76-mm-diameter filament is about 65.6 kΩ/m.[1] Typical lengths for the dipoles of these probes were $2h = 1.0$–5.0 cm. The miniature field probes recently developed for biological applications have dipoles which are much smaller in length, $2h = 1.5$–8.0 mm [4]–[7]. Both electrical and biological considerations require the dipoles to be at least this small. The conductors of the transmission lines for these miniature probes are formed by depositing a thin film of a metallic alloy on a dielectric substrate; a typical resistance per unit length being 1–10 MΩ/m. Current interest is in utilizing the technology of microwave integrated circuits to produce even smaller dipole probes ($2h \approx 0.5$ mm) for use in *in vivo* bioelectromagnetic dosimetry. When these probes are fully developed, they will have many applications in addition to those in the area of bioelectromagnetics. The design and the fabrication of the lossy transmission lines for these very small probes are critical, particularly if the performance of the combination of the dipole, diode, and transmission line is to be optimized. The empirical procedures used in the past may not be sufficient for this purpose.

It is the purpose of this paper to present theoretical electromagnetic analyses, supported by experimentation, for the combination of the electrically short dipole and the lossy transmission line. Specifically, i) the direct reception of the incident signal by the transmission line is evaluated and compared with that for the dipole, ii) the scattering of the incident signal by the transmission line is studied by formulating the scattering cross section for the line, and iii) the behavior of the lossy line as a low-pass filter is examined. The results of the analyses are presented as simple formulas that can be used for probe design and optimization.

Only the single dipole with a lossy transmission line in free space is examined. Methods for combining three dipoles to obtain an isotropic response and the special techniques, such as insulating the dipole, that are used to improve the response of the probe when immersed in a material medium are discussed in the literature [4]–[11].

II. Formulation of the Problem

Fig. 2 shows the model used in the analysis for the electric field probe. The dipole and the transmission line are orthogonal; the axis of the dipole is parallel to the z axis and the axis of the transmission line is parallel to the y axis. The dipole has half length h and conductor radius a_A, while the transmission line has length s, conductor radius a_L, and conductor spacing b. Lumped impedances Z_0 and Z_s (admittances Y_0 and Y_s) are connected at the ends of the

[1]This material is now commercially produced under the trade name Conductive Fluorosint by the Polymer Corporation, Reading, PA 19603.

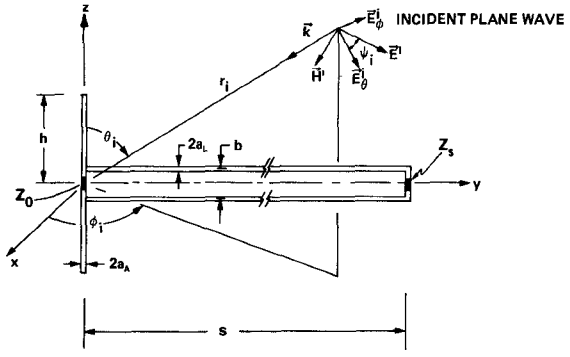

Fig. 2. Dipole with transmission line in incident plane wave field.

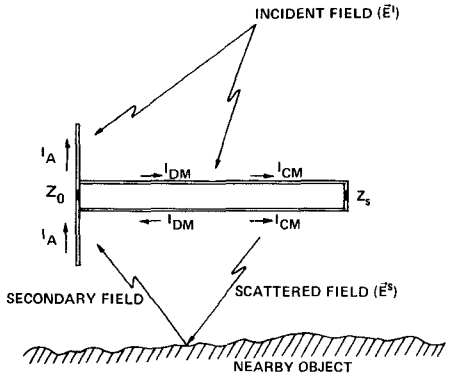

Fig. 3. Schematic diagram showing reception of incident signal.

transmission line, $y=0$ and $y=s$, respectively. In an actual probe, these elements would represent the linear high-frequency impedance of the diode and the input impedance of the monitoring instrumentation. Note that the discrete element low-pass filter in Fig. 1 is not included in the model, but it can be added easily if needed. The incident signal is a linearly polarized electromagnetic plane wave propagating in the direction specified by the angles θ_i, ϕ_i with the electric field

$$\boldsymbol{E}^i(\boldsymbol{r},\omega)=\boldsymbol{E}^i_\theta+\boldsymbol{E}^i_\phi=E^i\left(\cos\psi_i\hat{\theta}_i+\sin\psi_i\hat{\phi}_i\right)e^{-j\boldsymbol{k}\cdot\boldsymbol{r}} \quad (2)$$

where

$$\boldsymbol{k}\cdot\boldsymbol{r}=-\beta_0\left(x\sin\theta_i\cos\phi_i+y\sin\theta_i\sin\phi_i+z\cos\theta_i\right). \quad (3)$$

A complex harmonic time dependence $e^{j\omega t}$ is assumed, and $\beta_0=\omega\sqrt{\mu_0\epsilon_0}$ is the propagation constant for free space.

The incident wave produces currents in the dipole and in the transmission line. The current in the transmission line can be split into two components: the differential-mode current I_{DM}, which is equal in amplitude in the two conductors, but opposite in direction, and the common-mode current I_{CM}, which has equal amplitude and the same direction in both conductors, see Fig. 3. The differential-mode current I_{DM} goes through the terminal impedances Z_0 and Z_s and is responsible for the direct reception of the incident signal by the transmission line; the common-mode current is zero in the terminations. The common-mode current, however, is the source of the scattered electromagnetic field for the transmission line. The scattered field can produce currents in nearby objects, and these, in turn, can produce a secondary field received by the dipole or transmission line, see Fig. 3. Thus the currents I_{DM} and I_{CM} are the sources of two errors produced in the measurement, viz., the direct reception of the incident signal by the transmission line, and the scattering of the incident signal by the transmission line that can result in the reception of an erroneous signal by the probe.

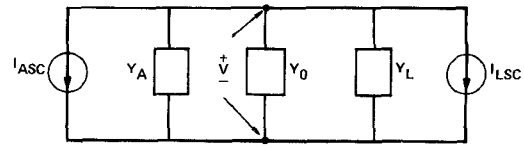

Fig. 4. Norton equivalent circuit for dipole-transmission-line reception.

In the study of the combination of the dipole and transmission line, the reception by the transmission line, i.e., the differential-mode current I_{DM} ($y=0$) in the impedance Z_0, is calculated and compared to the reception by the dipole antenna, i.e., the antenna current I_A ($z=0$) in the impedance Z_0. The degradation of the receiving pattern for the dipole by the transmission line is then examined. The effect of the scattering of the incident wave by the transmission line on the reception by the dipole cannot be completely assessed unless a description of all objects near the probe is provided. A measure of the effect, however, can be obtained by considering the general scattering properties of the transmission line and comparing these with the scattering properties of the dipole. This is done by formulating the total scattering cross section and the backscattering cross section for broadside incidence of the dipole and the transmission line separately.

In the analysis, the electromagnetic coupling between the dipole and the orthogonal transmission line is ignored, and the only interaction considered between these elements is at their connection.

III. Reception of the Incident Wave

The reception of the incident signal by the combination of the dipole and the transmission line is analyzed using the Norton equivalent circuit shown in Fig. 4. In this circuit, the current generators I_{ASC} and I_{LSC} are the currents that would be produced by the incident field in a short circuit at the terminals of the dipole and at the left terminals of the transmission line, respectively, and the admittances Y_A and Y_L are those for the driven dipole and the driven transmission line (the input admittance of the line terminated with the impedance Z_S). For an electrically short dipole ($\beta_0 h \ll 1$) the circuit elements are

$$I_{ASC}\approx -hE^i\cos\psi_i\sin\theta_i Y_A \quad (4)$$

$$Y_A\approx j\pi\beta_0 h/\zeta_0\left[\ln\left(h/a_A\right)-1\right] \quad (5)$$

where terms of order $(\beta_0 h)^2$ or less have been ignored, and $\zeta_0=\sqrt{\mu_0/\epsilon_0}$ is the impedance of free space [10]. The input admittance for the transmission line is simply

$$Y_L=Y_c\left[\frac{Y_s+jY_c\tan\left(k_L s\right)}{jY_s\tan\left(k_L s\right)+Y_c}\right] \quad (6)$$

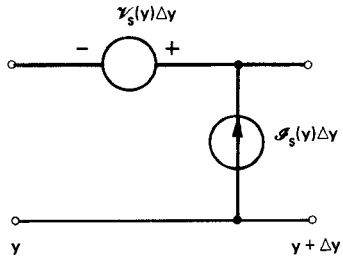

Fig. 5. Equivalent voltage and current sources for a length Δy of the transmission line.

where the complex wavenumber k_L and the characteristic admittance Y_c (impedance Z_c) are expressed in terms of the series impedance per unit length z_L and the shunt admittance per unit length y_L

$$k_L=\beta_L-j\alpha_L=\sqrt{-z_Ly_L} \tag{7}$$

$$Y_c=1/Z_c=\sqrt{y_L/z_L}\,. \tag{8}$$

The series impedance per unit length is the sum of the internal impedance per unit length of the conductors $2z^i$ and the impedance of the external inductance per unit length l^e

$$z_L=2z^i+j\omega l^e=2r^i+j\omega(2l^i+l^e) \tag{9}$$

and the shunt admittance per unit length is the sum of the conductance per unit length g, and the admittance of the capacitance, c, per unit length

$$y_L=g+j\omega c. \tag{10}$$

Note that the internal impedance per unit length of each conductor is z^i, requiring the factor of two in the loop impedance per unit length (9). It remains to determine the equivalent current generator for the transmission line I_{LSC} by analyzing the excitation of the line by the incident field.

The effect of the incident electromagnetic field on the transmission line is equivalent to a distributed series voltage source and a distributed shunt current source [12], [13], see Fig. 5. For a general incident field $\boldsymbol{E}^i(x, y, z)$, $\boldsymbol{B}^i(x, y, z)$, the equivalent voltage and current sources per unit length of the line are

$$\mathcal{V}_s(y)=j\omega\int_{-b/2}^{b/2}B_x^i(0, y, z)\,dz \tag{11}$$

and

$$\mathcal{I}_s(y)=-y_L\int_{-b/2}^{b/2}E_z^i(0, y, z)\,dz. \tag{12}$$

These sources appear on the right-hand sides of the transmission-line equations for the differential-mode voltage and current

$$\frac{\partial V_{\mathrm{DM}}(y)}{\partial y}+z_LI_{\mathrm{DM}}(y)=\mathcal{V}_s(y) \tag{13}$$

$$\frac{\partial I_{\mathrm{DM}}(y)}{\partial y}+y_LV_{\mathrm{DM}}(y)=\mathcal{I}_s(y). \tag{14}$$

After combining (11)–(14) and using Maxwell's equations, the following partial differential equations of the second order are obtained for the voltage and the current in the transmission line:

$$\frac{\partial^2V_{\mathrm{DM}}(y)}{\partial y^2}+k_L^2V_{\mathrm{DM}}(y)=y_L2z^i\int_{-b/2}^{b/2}E_z^i(0, y, z)\,dz+j\omega\int_{-b/2}^{b/2}\frac{\partial B_y^i(0, y, z)}{\partial x}dz \tag{15}$$

$$\frac{\partial^2I_{\mathrm{DM}}(y)}{\partial y^2}+k_L^2I_{\mathrm{DM}}(y)=y_L\left[E_y^i(0, y, b/2)-E_y^i(0, y, -b/2)\right]. \tag{16}$$

The solution of the differential system consisting of (15), (16), and the boundary conditions $V_{\mathrm{DM}}(0)=-Z_0I_{\mathrm{DM}}(0)$, $V_{\mathrm{DM}}(s)=Z_sI_{\mathrm{DM}}(s)$ is straightforward [12], [13]. Specifically, the solution for the current at the left termination of the line, $y=0$, is

$$I_{\mathrm{DM}}(0)=\Big\{\left[j\bar{Z}_s\sin k_Ls+\cos k_Ls\right]\cdot\int_{-b/2}^{b/2}E_z^i(0,0,z)\,dz-\int_{-b/2}^{b/2}E_z^i(0,s,z)\,dz-\int_0^s\left[E_y^i(0,y,b/2)-E_y^i(0,y,-b/2)\right]\cdot\left[j\bar{Z}_s\sin k_L(y-s)-\cos k_L(y-s)\right]dy\Big\}/Z_cD \tag{17}$$

where

$$D=j(1+\bar{Z}_0\bar{Z}_s)\sin k_Ls+(\bar{Z}_0+\bar{Z}_s)\cos k_Ls \tag{18}$$

and the normalized impedance $\bar{Z}$ (admittance $\bar{Y}$) is $\bar{Z}=Z/Z_c$ ($\bar{Y}=Y/Y_c$). When the incident field (2) is substituted into (17), the inequality $\beta_0b\ll1$ used, and the integrals evaluated, the current becomes

$$\begin{aligned}I_{\mathrm{DM}}(0)=(E^ib/Z_c)\Big\{&\cos\theta_i\Big[\left(\cos k_Ls-e^{j\beta_0s\sin\theta_i\sin\phi_i}\right)\left(\sin\theta_i\sin\phi_i+\bar{k}_L\bar{Z}_s\right)\\&+j\sin k_Ls\left(\bar{Z}_s\sin\theta_i\sin\phi_i+\bar{k}_L\right)\Big]\\&\cdot\left[\cos\theta_i\sin\phi_i\cos\psi_i+\cos\phi_i\sin\psi_i\right]/\left(\bar{k}_L^2-\sin^2\theta_i\sin^2\phi_i\right)\\&-\sin\theta_i\left[j\bar{Z}_s\sin k_Ls+\cos k_Ls-e^{jb_0s\sin\theta_i\sin\phi_i}\right]\\&\cdot\cos\psi_i\Big\}/D\end{aligned} \tag{19}$$

where $\bar{k}_L=k_L/\beta_0$. The current generator I_{LSC}, which appears in the Norton equivalent circuit of Fig. 4, is determined by setting Z_0 equal to zero in (19)

$$I_{LSC}=I_{\mathrm{DM}}(0)|_{Z_0=0}. \tag{20}$$

With the values of elements in the equivalent circuit of Fig. 4 given by (4)–(6) and (20), the oscillating voltage V

across the terminals of the load impedance Z_0 (admittance Y_0) is determined

$$V=-(I_{ASC}+I_{LSC})/(Y_A+Y_L+Y_0). \tag{21}$$

From this equation it is seen that the relative reception of the incident field by the dipole and the transmission line can be evaluated by comparing the two components of the total short-circuit current $I_{TSC}=I_{ASC}+I_{LSC}$. For the special case of interest, the high loss per unit length of the transmission line introduces the inequality

$$|e^{-jk_L s}|=e^{-\alpha_L s}\ll 1 \tag{22}$$

which simplifies greatly the expressions for the current I_{LSC} and the admittance Y_L

$$\begin{aligned} I_{LSC}\approx &\left(E^i b/Z_c\right)\left[\cos\theta_i(\cos\theta_t\sin\phi_t\cos\psi_t\right.\\ &+\cos\phi_t\sin\psi_t)/(\bar{k}_L-\sin\theta_i\sin\phi_i)\\ &\left.-\sin\theta_t\cos\psi_t\right] \end{aligned} \tag{23}$$

$$Y_L\approx Y_c. \tag{24}$$

After combining (4) and (23), the total short-circuit current becomes

$$\begin{aligned} I_{TSC}\approx &\frac{-j\pi\omega\epsilon_0 h^2 E^i}{\ln(h/a_A)-1}\left\{\sin\theta_t\cos\psi_t\right.\\ &-\chi\left[\cos\theta_i(\cos\theta_t\sin\phi_t\cos\psi_t\right.\\ &+\cos\phi_t\sin\psi_t)/(1-\sin\theta_i\sin\phi_i/\bar{k}_L)\\ &\left.\left.-\bar{k}_L\sin\theta_t\cos\psi_t\right]\right\} \end{aligned} \tag{25}$$

where the parameter χ is

$$\chi=\frac{\ln(h/a_A)-1}{\pi}(b/h)(\zeta_0/z_L h). \tag{26}$$

Note that after the use of (22), the current I_{TSC} is independent of the length s of the transmission line and the load impedance Z_s.

Additional simplification of (25) is possible if assumptions are made concerning the impedance z_L and the admittance y_L per unit length of the transmission line. For a line with negligible conductance per unit length $g\approx 0$ and a high resistance per unit length $2r^i\gg\omega(2l^i+l^e)$

$$z_L\approx 2r^i \qquad y_L\approx j\omega c \tag{27}$$

which makes

$$\bar{k}_L\approx\sqrt{-j\omega 2r^i c}\,/\beta_0=\sqrt{r^i/\omega l^e}\,(1-j) \tag{28a}$$

thus

$$|\bar{k}_L|\gg 1. \tag{28b}$$

With these results, (25) becomes

$$\begin{aligned} I_{TSC}\approx &\frac{-j\pi\omega\epsilon_0 h^2 E^i}{\ln(h/a_A)-1}\left\{F_A(\theta_t)\cos\psi_t\right.\\ &-\chi\left[F_{L1}(\theta_i,\phi_i)\cos\psi_t+F_{L2}(\theta_i,\phi_i)\sin\psi_t\right.\\ &\left.\left.-\bar{k}_L F_A(\theta_i)\cos\psi_t\right]\right\} \end{aligned} \tag{29}$$

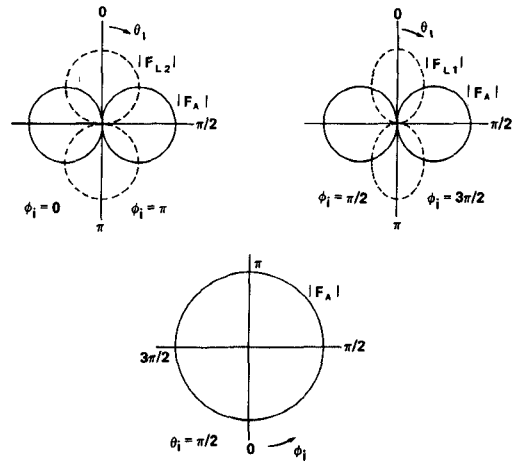

Fig. 6. Polar field patterns in principal planes for functions $F_A(\theta_t,\phi_t)$, $F_{L1}(\theta_t,\phi_t)$, and $F_{L2}(\theta_t,\phi_t)$.

where

$$F_A(\theta_t)=\sin\theta_t \tag{30a}$$

$$F_{L1}(\theta_t,\phi_t)=\cos^2\theta_t\sin\phi_t \tag{30b}$$

$$F_{L2}(\theta_t,\phi_t)=\cos\theta_t\cos\phi_t \tag{30c}$$

and

$$\chi\approx\frac{\ln(h/a_A)-1}{\pi}(b/h)(\zeta_0/2r^i h). \tag{31}$$

The first term in the braces in (29) results from the reception of the incident field by the electrically short dipole antenna, the remainder, i.e., the terms with the coefficient χ, is due to the reception by the transmission line. A careful examination of these terms will indicate the effect of the transmission line on the response of the electric field probe. The response of the dipole antenna, specified by the function $F_A(\theta_i)$, is to the $\hat{\theta}_i$ component of the incident electric field, and it has the familiar figure-eight shaped polar field pattern shown in Fig. 6. The response of the transmission line has three terms, the last of these has the same form as the response for the dipole, $F_A(\theta_i)$, and simply contributes to the desired response for the probe. The other two terms are responses to the $\hat{\theta}_i$ and $\hat{\phi}_i$ components of the incident field and are proportional to the functions $F_{L1}(\theta_i,\phi_i)$ and $F_{L2}(\theta_i,\phi_i)$, respectively. The former causes the pattern for the probe to deviate from that for the dipole, particularly in the vicinity of the nulls, and the latter causes the probe to respond to an electric field orthogonal to the dipole. Polar patterns for the functions $F_{L1}(\theta_i,\phi_t)$ and $F_{L2}(\theta_i,\phi_i)$ in the principal planes are shown in Fig. 6.

For purposes of discussion, it is convenient to combine the terms proportional to $F_A(\theta_t,\phi_i)$ in (29) and introduce the normalized current $\bar{I}_{TSC}$

$$\begin{aligned} \bar{I}_{TSC}&=I_{TSC}/\left\{-j\omega\epsilon_0 h^2(1+\bar{k}_L\chi)E^i/[\ln(h/a_A)-1]\right\}\\ &=F_A(\theta_t)\cos\psi_t-\bar{\chi}\left[F_{L1}(\theta_t,\phi_t)\cos\psi_t\right.\\ &\quad\left.+F_{L2}(\theta_i,\phi_t)\sin\psi_i\right] \end{aligned} \tag{32}$$

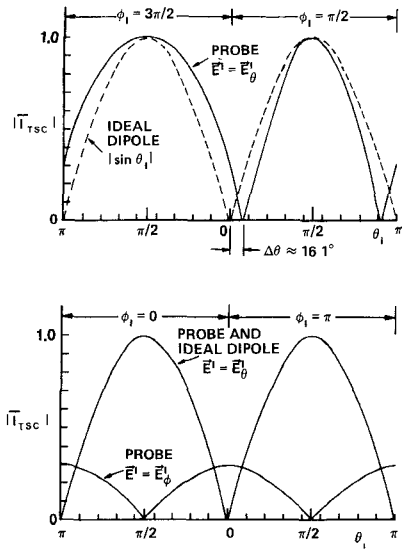

Fig. 7. Rectangular field patterns in principal planes for probe with parameter $\chi=0.3$. (a) $\phi_i=\pi/2, 3\pi/2$. (b) $\phi_i=0, \pi$.

where

$$\bar{\chi}=\chi/(1+\bar{k}_L\chi)$$
$$=\chi/\{1+(b/h)(\bar{k}_L\zeta_0/2r'h)[\ln(h/a_A)-1]/\pi\}. \quad (33)$$

The deviation of the normalized response of the probe (32) from that of the ideal dipole, the error in the response, is simply proportional to the complex parameter $\bar{\chi}$ (33). The magnitude of this parameter is always less than the real parameter χ (31), $|\bar{\chi}|\leq\chi$, and for many practical designs $|\bar{k}_L\chi|\ll 1$, so that $\bar{\chi}\approx\chi$. Therefore, the real parameter χ is a useful measure of the error in the response of the probe. Note that the product of the dimensionless ratios (b/h) and $(\zeta_0/r'h)$ appears in the expression for χ. Thus if the length h of the dipole in a probe is to be reduced by a factor ξ without increasing the error (χ) in the response, the spacing between the conductors of the transmission line must be decreased by the factor ξ *and* their resistance per unit length must be increased by the factor $1/\xi$. Alternatively, only the spacing or the resistance need be changed, but then by the factors ξ^2 and $(1/\xi)^2$, respectively. Note that χ is not a function of the frequency when the resistance per unit length r' is frequency independent.

To illustrate the error introduced in the response of the probe by the transmission line, rectangular field patterns are shown in Fig. 7 for a probe with the parameter $\chi=0.3$ $(|\bar{k}_L\chi|\ll 1)$. The reception by the transmission line is seen to cause the pattern of the probe in the plane $\phi_i=\pi/2$, $3\pi/2$ for an incident field $\boldsymbol{E}^i_\theta$, Fig. 7(a), to deviate from that of the ideal dipole $|\sin\theta_i|$. The width of the lobe in the half plane $\phi_i=\pi/2$ is decreased, while the width of the lobe in the half plane $\phi_i=3\pi/2$ is increased. The nulls in the pattern are shifted by approximately the amount

$$\Delta\theta=\sin^{-1}\left[\left(\sqrt{1+4\chi^2}-1\right)/2\chi\right]\approx\chi, \qquad \chi\ll 1 \quad (34)$$

which for this example is about 16.1°. In the plane $\phi_i=0, \pi$, the pattern of the probe for an incident field $\boldsymbol{E}^i_\theta$, Fig. 7(b), is the same as that of an ideal dipole; however, there is a response to an incident field $\boldsymbol{E}^i_\phi$ that does not exist for the ideal dipole.

IV. Scattering of the Incident Wave

The currents produced in the dipole antenna and the transmission line by the incident field are the sources of the secondary or scattered field. With reference to Fig. 3, the current I_A is the source of the scattered field for the dipole antenna. At distances from the transmission line that are large compared to the spacing of the conductors b, the field of the common-mode current I_{CM} is much greater than that of the differential-mode current I_{DM}. Thus the common-mode current I_{CM} is the major source of the scattered field for the transmission line. In the analysis of the scattering from the probe, the scattering from the dipole antenna and the transmission line will be evaluated separately and compared. As in the analysis of the reception by the probe, Section III, the electromagnetic coupling between the dipole and the orthogonal transmission line is ignored.

The scattering cross sections are convenient quantities for comparing the relative scattering from the dipole and transmission line and for studying the effect of parameters, such as the resistance per unit length of the transmission line, on the scattering. The cross sections considered are the total scattering cross section σ, which is the ratio of the total time-average power scattered P^s to the time-average power density of the incident wave S^i

$$\sigma(\theta_i,\phi_i;\psi_i)=P^s/S^i \quad (35)$$

and the backscattering cross section σ_B, which is the ratio

$$\sigma_B(\theta_i,\phi_i;\psi_i)=P^s_{\text{isotropic}}/S^i \quad (36)$$

where $P^s_{\text{isotropic}}$ is the total time-average power radiated by an isotropic scatterer that maintains the same electromagnetic field in all directions as maintained by the actual scatterer in the direction (θ_i,ϕ_i) toward the source [14]. The total scattering cross section in terms of the incident and scattered electric fields $\boldsymbol{E}^i$ and $\boldsymbol{E}^s$ is

$$\sigma(\theta_i,\phi_i;\psi_i)=\lim_{r\to\infty}\frac{\int\int \boldsymbol{E}^s\cdot(\boldsymbol{E}^s)^* r^2\,d\Omega}{\boldsymbol{E}^i\cdot(\boldsymbol{E}^i)^*}$$
$$=\lim_{r\to\infty}\frac{\int\int\left(|E^s_\theta|^2+|E^s_\phi|^2\right)r^2\,d\Omega}{|E^i|^2} \quad (37)$$

where $d\Omega$ is the element of solid angle for a sphere of radius r that completely encloses the scatterer. The backscattering cross sections considered are those for an incident wave broadside to the dipole or transmission line with the electric field parallel to the conductors. For the dipole antenna $(\theta_i=\pi/2, \phi_i=0; \psi_i=0)$

$$\sigma_{BA}=\sigma_B(\pi/2,0;0)=\lim_{r\to\infty}\frac{4\pi r^2|E^s_\theta(\theta=\pi/2,\phi=0)|^2}{|E^i|^2} \quad (38)$$

and for the transmission line ($\theta_i=0, \phi_i=\pi/2; \psi_i=0$)

$$\sigma_{BL}=\sigma_B(0,\pi/2;0)=\lim_{r\to\infty}\frac{4\pi r^2|E_\theta^s(\theta=0,\phi=\pi/2)|^2}{|E^i|^2}. \tag{39}$$

When normalized to the square of the free-space wavelength λ_0, the well-known cross sections for the electrically short dipole with its terminals short circuited ($Z_0=0$) are the total cross section [15]

$$\sigma_A(\theta_i;\psi_i)/\lambda_0^2 = 2(\beta_0 h)^6\sin^2\theta_i\cos^2\psi_i/\left\{27\pi\left[\ln(h/a_A)-1\right]^2\right\} \tag{40}$$

and the backscattering cross section[2]

$$\sigma_{BA}/\lambda_0^2=(\beta_0 h)^6/\left\{9\pi\left[\ln(h/a_A)-1\right]^2\right\}. \tag{41}$$

Before the cross sections for the transmission line can be evaluated, the common-mode current distribution $I_{CM}(y)$ and the field that it produces $\boldsymbol{E}^s$ must be determined. The common-mode current in each conductor is a solution to the following approximate integral equation:

$$\int_0^s\left[I_{CM}(y')e^{-j\beta_0 R_e}/R_e\right]dy' - j\beta_0\bar{z}^i\int_0^y I_{CM}(y')\sin\beta_0(y-y')\,dy' = \frac{-j\lambda_0 E^i(\cos\psi_i\cos\theta_i\sin\phi_i+\sin\psi_i\cos\phi_i)}{\zeta_0(1-\sin^2\theta_i\sin^2\phi_i)} \cdot e^{j\beta_0 y\sin\theta_i\sin\phi_i}+A\cos\beta_0 y+B\sin\beta_0 y \tag{42}$$

where A and B are constants to be determined by the end conditions $I_{CM}(0)=I_{CM}(s)=0$, and the normalized internal impedance per unit length is

$$\bar{z}^i=z^i\lambda_0/\zeta_0. \tag{43}$$

This is the familiar integral equation for the current on a thin-wire scatterer with the equivalent radius

$$a_e=\sqrt{a_L b} \tag{44}$$

appearing in the distance R_e

$$R_e=\left[(y-y')^2+a_e^2\right]^{1/2}. \tag{45}$$

The equivalent radius approximately accounts for the fact that the transmission line is composed of two closely spaced conductors ($\beta_0 b\ll 1$) carrying equal currents rather than a single conductor [16]. The integral equation (42) can be solved for the current by any of a number of straightforward numerical methods and the scattered field and cross sections determined [17]. Typical results are shown in Fig. 8 for the normalized total scattering cross section σ_L/λ_0^2 of a one-wavelength-long transmission line ($s=\lambda_0, a_e=3.33\times10^{-3}\lambda_0$) with the incident field from the direction $\theta_i=0$, $\phi_i=\pi/2$ and with the polarization $\psi_i=0$ (E_θ^i component only). The cross section is shown as a function of the normalized internal resistance per unit length of the conductors $\bar{r}^i=r^i\lambda_0/\zeta_0$, and it is seen to be reduced significantly by an increase in the resistance once $\bar{r}^i$ is greater than about 10. The three regions marked on the graph represent typical ranges of σ_L/λ_0^2 at a frequency of 1 GHz for metallic wires with a radius $a_L=25$ μm (1 mil), the NBS carbon–Teflon conductor, and thin-metallic-film conductors. From this graph, it is clear why the high-resistance transmission lines are often referred to as "transparent" to electromagnetic fields at high radio and microwave frequencies.

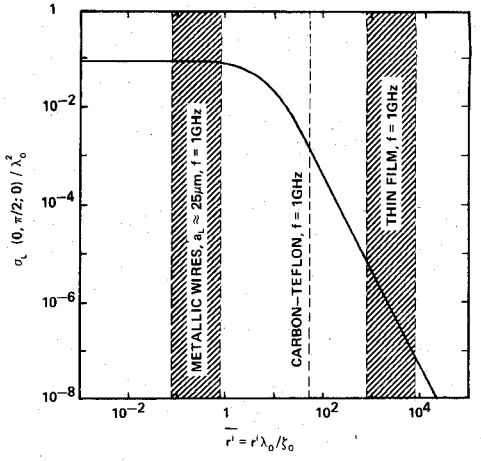

Fig. 8. Normalized total scattering cross section of a one-wavelength-long transmission line ($s/\lambda_0=1.0, a_e/\lambda_0=3.33\times10^{-3}$) for an incident wave with $\theta_i=0, \phi_i=\pi/2$, and $\psi_i=0$.

While numerical methods can provide an accurate solution to the integral equation (42) for specific values of the parameters, an analytic solution to the equation is more useful in performing parametric studies. An analytic expression for the current $I_{CM}(y)$ can be obtained by approximating the integral equation for the special case of interest, namely, conductors with a high internal impedance per unit length. The first integral on the left of (42) has a kernel with a sharp peak at the point $y=y'$. This behavior is often used in antenna theory to replace this integral by the term $\psi I_{CM}(y)$ and obtain the so-called "zeroth-order" solution to the equation [16]. The particular choice of the constant ψ is not important for the purposes of the following argument, but an estimate of its magnitude can be obtained from the value for an electrically short antenna $\psi=2\ln(s/a_e)-2$. With this substitution, the approximate integral equation becomes

$$I_{CM}(y)-\frac{j\beta_0\bar{z}^i}{\psi}\int_0^y I_{CM}(y')\sin\beta_0(y-y')\,dy' \approx \frac{-jE^i\lambda_0(\cos\psi_i\cos\theta_i\sin\phi_i+\sin\psi_i\cos\phi_i)}{\zeta_0\psi(1-\sin^2\theta_i\sin^2\phi_i)} \cdot e^{j\beta_0 y\sin\theta_i\sin\phi_i}+A'\cos\beta_0 y+B'\sin\beta_0 y. \tag{46}$$

This is a Volterra integral equation of the second kind with

[2] These formulas differ from those of [15] in that the term $\ln(4h/a_A)$ is replaced by $\ln(h/a_A)$.

a convolution-type kernel; its solution is easily obtained using the Laplace transformation [18]

$$I_{CM}(y)=\frac{-jE^i\lambda_0(\cos\theta_i\sin\phi_i\cos\psi_i+\cos\phi_i\sin\psi_i)}{\zeta_0\psi(1-\sin^2\theta_i\sin^2\phi_i-j\bar{z}^i/\psi)}\cdot\left\{e^{j\beta_0 y\sin\theta_i\sin\phi_i}-\left[\sin k_s(s-y)+\sin k_s y\cdot e^{j\beta_0 s\sin\theta_i\sin\phi_i}\right]/\sin k_s s\right\} \quad (47)$$

transmission line is

$$E^s=-j\omega\mu_0(\hat{\theta}\cos\theta\sin\phi+\hat{\phi}\cos\phi)\frac{e^{-j\beta_0 r}}{4\pi r}\cdot 2\int_0^s I_{CM}(y')e^{j\beta_0 y'\sin\theta\sin\phi}\,dy' \quad (55)$$

which, on substitution of (54) and evaluation of the integral, becomes

$$E^s\approx\frac{-jE^i\lambda_0(\cos\theta_i\sin\phi_i\cos\psi_i+\cos\phi_i\sin\psi_i)\sin\left[\beta_0 s(\sin\theta_i\sin\phi_i+\sin\theta\sin\phi)/2\right]}{\pi r\bar{z}_i(\sin\theta_i\sin\phi_i+\sin\theta\sin\phi)e^{-j\beta_0 r}e^{j\beta_0 s(\sin\theta_i\sin\phi_i+\sin\theta\sin\phi)/2}(\hat{\theta}\cos\theta\sin\phi+\hat{\phi}\cos\phi)}. \quad (56)$$

where

$$k_s=\beta_s-j\alpha_s=\beta_0(1-j\bar{z}^i/\psi)^{1/2}. \quad (48)$$

For the lossy transmission lines of interest, the resistance per unit length is high enough to make

$$|\bar{z}^i/\psi|=|z^i\lambda_0/\zeta_0\psi|\gg 1 \quad (49)$$

$$k_s\approx\beta_0\sqrt{\bar{z}^i/2\psi}\,(1-j). \quad (50)$$

In addition, the attenuation of a wave propagating along the length of the line s is large

$$|e^{-jk_s s}|=e^{-\alpha_s s}\ll 1. \quad (51)$$

This last inequality follows from (22), since

$$\alpha_s s\approx\alpha_L s\sqrt{\psi\zeta_0/2\pi Z_{c0}} \quad (52)$$

where Z_{c0} is the characteristic impedance of the transmission line when the conductors have zero internal impedance per unit length. The argument of the square root in (52) is usually of the order of unity; this can be seen by substituting the value of ψ for a short antenna and the value of Z_{c0} for a two-wire transmission line

$$\psi\zeta_0/2\pi Z_{c0}\approx\left[\ln(s/a_e)-1\right]/\ln(b/a_L). \quad (53)$$

This ratio of logarithmic terms is usually less than five for practical geometries. Thus when the inequality (22) applies to $\alpha_L s$, the inequality (52) for $\alpha_s s$ also holds. After using (49) and (51), the current (47) is approximately

$$I_{CM}(y)\approx(E^i/z^i)(\cos\theta_i\sin\phi_i\cos\psi_i+\cos\phi_i\sin\psi_i)\cdot\left\{e^{j\beta_0 y\sin\theta_i\sin\phi_i}-e^{-jk_s y}+e^{-jk_s(s-y)}e^{j\beta_0 s\sin\theta_i\sin\phi_i}\right\}$$
$$\approx(E^i/z^i)(\cos\theta_i\sin\phi_i\cos\psi_i+\cos\phi_i\sin\psi_i)\cdot e^{j\beta_0 y\sin\theta_i\sin\phi_i}. \quad (54)$$

The last line in (54) is obtained by recognizing that terms with $-k_s$ in the exponent can be neglected, because they are only significant at points very close to the ends of the transmission line ($y=0, s$) when (51) is satisfied. Note, that to this degree of approximation, the current is independent of the parameter ψ.

The scattered electric field E^s in the far zone of the

The total scattering cross section σ_L and the backscattering cross section σ_{BL} for the transmission line are obtained by using (56) in (37) and (39). After performing the surface integration in (37) and rearranging terms, the normalized total scattering cross section becomes

$$\sigma_L(\theta_i,\phi_i,\psi_i)/\lambda_0^2\approx(2/\pi|\bar{z}^i|^2)|\cos\theta_i\sin\phi_i\cos\psi_i+\cos\phi_i\sin\psi_i|^2\cdot\Big[(1/\beta_0 s)\sin\beta_0 s\cos(\beta_0 s\sin\theta_i\sin\phi_i)-2+\sin\theta_i\sin\phi_i\sin\beta_0 s\cdot\sin(\beta_0 s\sin\theta_i\sin\phi_i)+\cos\beta_0 s\cos(\beta_0 s\sin\theta_i\sin\phi_i)+\sin\theta_i\sin\phi_i\{\mathrm{Cin}[\beta_0 s(1+\sin\theta_i\sin\phi_i)]-\mathrm{Cin}[\beta_0 s(1-\sin\theta_i\sin\phi_i)]\}+(\beta_0 s/2)(1-\sin^2\theta_i\sin^2\phi_i)\cdot\{\mathrm{si}[\beta_0 s(\sin\theta_i\sin\phi_i+1)]-\mathrm{si}[\beta_0 s(\sin\theta_i\sin\phi_i-1)]\}\Big] \quad (57)$$

where $\mathrm{si}(x)$ and $\mathrm{Cin}(x)$ are the sine and cosine integrals [19]

$$\mathrm{si}(x)=\mathrm{Si}(x)-\pi/2=-\int_0^{\pi/2}e^{-x\cos t}\cos(x\sin t)\,dt \quad (58)$$

$$\mathrm{Cin}(x)=-\mathrm{Ci}(x)+\ln(x)+\gamma=-\int_0^x(\cos t-1)/t\,dt \quad (59)$$

and γ is Euler's constant. The normalized backscattering cross section is simply

$$\sigma_{BL}/\lambda_0^2\approx(\beta_0 s/|\bar{z}^i|)^2/\pi=\left[\beta_0 s/(|z^i|\lambda_0/\zeta_0)\right]^2/\pi. \quad (60)$$

The normalized total scattering cross section $(\sigma_L/\lambda_0^2)/(\beta_0 s/|\bar{z}^i|^2)$ computed from (57) is shown in Fig. 9 as a function of the electrical length $\beta_0 s$ of the transmis-

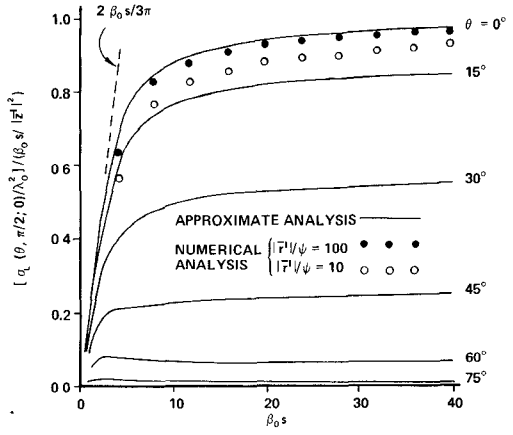

Fig. 9. Normalized total scattering cross section for transmission line as a function of the electrical length $\beta_0 s$, $\phi_i = \pi/2$, $\psi_i = 0$.

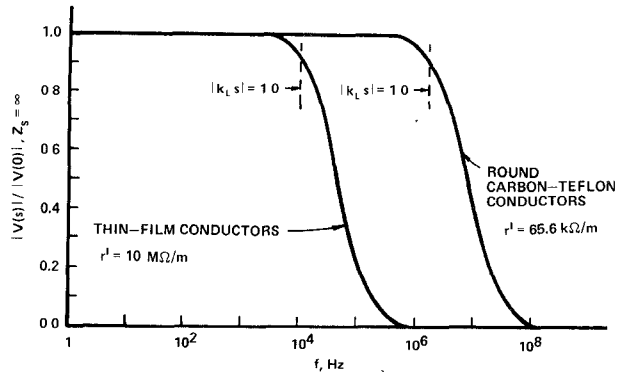

Fig. 10. The operation of the transmission line as a low-pass filter, the voltage ratio $|V(s)|/|V(0)|$ as a function of frequency for resistive transmission lines terminated in an open circuit, $Z_s = \infty$.

sion line. The incident wave for this example is in the plane $\phi_i = \pi/2$ with the electric field in the direction $\hat{\theta}_i$ ($\psi_i = 0$); the angle θ_i is the parameter on the graph. This orientation and polarization for the incident wave provides a complete description of the scattering, since the scattering by the line is rotationally symmetric about the y axis as a result of approximating the two conductors of the line by one of equivalent radius, and only the component of the incident electric field that is parallel to the y axis is scattered by the line. Two sets of cross sections computed from the numerical solution of the integral equation (42) are also shown in Fig. 9. These are for an angle of incidence $\theta_i = 0°$ and two values of the normalized resistance per unit length, $|\bar{r}^i|/\psi = 10$, 100, where ψ is taken to be $\psi = 2\ln(s/a_e) - 2$. As expected, the total scattering cross sections obtained using the approximate formula (57) are in good agreement with those from the numerical analysis when the parameter $|\bar{r}^i|/\psi$ is large.

The maximum cross section for any of the lengths $\beta_0 s$ shown in Fig. 9 occurs when the angle of incidence is $\theta_i = 0$

$$\sigma_L(0, \pi/2; 0)/\lambda_0^2 = (2/\pi|\bar{z}^i|^2)\left[(1/\beta_0 s)\sin\beta_0 s - 2 + \cos\beta_0 s + \beta_0 s\,\mathrm{Si}(\beta_0 s)\right]. \quad (61)$$

For electrically short lines $\beta_0 s \ll 1$, the total cross section is approximately

$$\sigma_L(0, \pi/2; 0)/\lambda_0^2 \approx 2(\beta_0 s)^2/(3\pi|\bar{z}^i|^2) \quad (62)$$

and for electrically long lines $\beta_0 s \gg 1$, the total cross section approaches

$$\sigma_L(0, \pi/2; 0)/\lambda_0^2 \approx \beta_0 s/|\bar{z}^i|^2 \quad (63)$$

see Fig. 9. The asymptotic value given in (63) is useful as an upper bound for the total scattering cross section of the lossy transmission line for all angles of incidence and polarizations of the incident wave.

The approximate formulas for the cross sections (57), (60), (62), and (63) can be used to study the effect of various parameters, such as the resistance per unit length r^i and the frequency, on the scattering by the lossy transmission line. A relative measure of the scattering is obtained by comparing these cross sections with those for the dipole antenna in the probe, (40) and (41). For example, a comparison can be made of the total scattering from the dipole and from a length of the transmission line equal to the length of the dipole, i.e., the ratio $(\sigma_L/s)/(\sigma_A/2h)$. If the maximum values of the total cross section for the line (61) and for the dipole (40), with $\theta_i = \pi/2$, $\psi_i = 0$, are used, this ratio becomes

$$\frac{\sigma_L(0, \pi/2; 0)/s}{\sigma_A(\pi/2; 0)/2h} = \frac{54(h/s)}{|\bar{z}^i|^2(\beta_0 h)^6}\left[(1/\beta_0 s)\sin\beta_0 s - 2 + \cos\beta_0 s + \beta_0 s\,\mathrm{Si}(\beta_0 s)\right]\left[\ln(h/a_A) - 1\right]^2. \quad (64)$$

For an internal impedance per unit length that is approximately a frequency-independent resistance $z^i \approx r^i$, the right side of (64) is inversely proportional to the square of the frequency when the line is electrically short ($\beta_0 s \ll 1$), and inversely proportional to the cube of the frequency when the line is electrically long ($\beta_0 s \gg 1$).

V. The Transmission Line as a Low-Pass Filter

The highly resistive transmission lines used in miniature field probes are very dispersive, i.e., the phase velocity for a wave propagating on the line is a strong function of the frequency. This is illustrated in Fig. 10 where the voltage transmission ratio

$$|V(s)/V(0)| = |\sec(k_L s)| \quad (65)$$

for the transmission line terminated in an open circuit, $Z_s = \infty$, is graphed as a function of the frequency. Results are shown for 20-cm-long lines formed from carbon–Teflon conductors ($r^i = 65.6$ kΩ/m) and thin-film conductors ($r^i = 10$ MΩ/m); the capacitance per unit length of both lines is $c = 20$ pF/m. The transmission ratio is seen to drop sharply once the frequency exceeds the point where $|k_L s| = 1$. For the carbon–Teflon conductors, this occurs at about $f = 1.5$ MHz and for the thin-film conductors at about $f = 10$ kHz.

Consider a probe, like that shown in Fig. 1, which is to

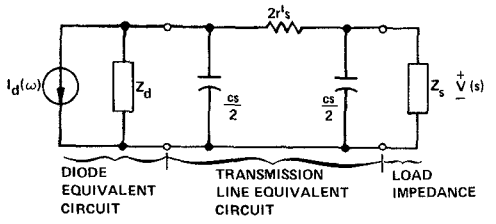

Fig. 11. Low-frequency output circuit for diode, transmission line, and termination, Z_s.

measure amplitude-modulated incident electric fields of the form

$$\boldsymbol{E}^i(\boldsymbol{r},t)=\boldsymbol{E}^i(\boldsymbol{r})f(t)\cos\left[\omega_0 t+\phi(\boldsymbol{r})\right]. \tag{66}$$

The modulating signal $f(t)$ in (66) in band limited, i.e., its Fourier transform $F(\omega)$ is zero above the frequency ω_m

$$F(\omega)=0, \qquad |\omega|>\omega_m. \tag{67}$$

The dipole antenna of the probe receives the incident signal (66) and impresses a voltage proportional to it across the diode. The nonlinear characteristic of the diode produces a current $i_d(t)$ proportional to the square of the amplitude modulation on the incident signal

$$i_d(t)=C|f(t)|^2. \tag{68}$$

The Fourier transform of this current $I_d(\omega)$ is also band limited

$$I_d(\omega)=0, \qquad |\omega|>2\omega_m. \tag{69}$$

For the transmission line to pass this current to the monitoring instrumentation without distortion, the frequency $2\omega_m$ must be below the frequency where $|k_L(\omega)s|=1$. As discussed earlier, the inequality $|k_L(\omega_0)s|\gg 1$ must be satisfied at the high radio or microwave carrier frequency ω_0 to minimize the perturbation in the reception produced by the transmission line. Thus with reference to Fig. 10, for proper operation of the probe, the carrier frequency ω_0 of the incident signal must be well above the point where $|k_L s|=1.0$, while the frequencies contained in the square of the modulating signal ($\omega\leqslant 2\omega_m$) must be below this point.

When the parameters for the transmission line and the modulation are selected so that the inequality

$$|k_L(\omega)s|^2\approx\omega c 2r's^2\ll 1 \tag{70}$$

is satisfied at the frequencies $\omega\leqslant 2\omega_m$, the resistive transmission line can be represented by the equivalent "Pi" network shown in Fig. 11. The other elements in this circuit diagram are the low-frequency Norton equivalent circuit for the output of the diode and the input impedance of the monitoring instrumentation Z_s. In the diode, equivalent circuit $I_d(\omega)$ is the short-circuit output current and Z_d the diode "video impedance," often take to be a resistance, viz., R_v the video resistance.[3] An expression for the voltage $V(s)$ at the input to the monitoring instrumentation is obtained from the equivalent circuit in Fig. 11. When the inequality (70) is used to simplify this expression, the voltage is approximately

$$\begin{aligned}V(s)&\approx -I_d Z_s Z_d/\left(Z_d+Z_s+2r's+j\omega csZ_dZ_s\right)\\&=-I_dZ_sZ_d/\left\{2r's\left(1+Z_d/2r's\right)\right.\\&\quad\left.+Z_s\left[1-j(k_Ls)^2\left(Z_d/2r's\right)\right]\right\}.\end{aligned} \tag{71}$$

For a practical probe, the resistance of the transmission line $2r's$ is usually much greater than the diode impedance

$$|Z_d/2r's|\ll 1. \tag{72}$$

After using the inequalities (70) and (72), (71) becomes

$$V(s)\approx -I_dZ_sZ_d/\left[2r's+Z_s\right]. \tag{73}$$

To summarize the results of this section, the resistive transmission line in the field probe behaves as a low-pass filter. If the probe is to be used to measure an amplitude-modulated field without distortion, the frequencies in the square of the modulating signal must lie within the passband of the transmission line, i.e., (70) must be satisfied for all frequencies $\omega\leqslant 2\omega_m$. The voltage across the input impedance Z_s of the monitoring instrumentation is then simply determined from (71) or (73).

VI. Comparison with Experiment

The previously obtained theoretical results show that the transmission line with finite resistance will distort the field pattern of the electric field probe from that of an ideal electrically short dipole. To verify these results, a model probe was constructed with the dimensions $h=1.25$ cm, $b=5.0$ mm, $a_A=0.19$ mm, $a_L=0.38$ mm, and $s=15.0$ cm. The conductors of the resistive transmission line were the NBS designed carbon–Teflon filament, $r'=65.6$ kΩ/m. At the frequency used for the measurements, $f=800$ MHz, the inequality (22) was satisfied, $e^{-\alpha_L s}=1.8\times 10^{-3}$, making the reception by the probe independent of the length of the transmission line and the load impedance Z_s.

The probe was placed in an approximately plane electromagnetic wave with electric field $\boldsymbol{E}^i_\theta$ in the plane formed by the dipole and transmission line ($\phi_i=\pi/2, 3\pi/2$), see Fig. 12(a). A field pattern was obtained by monitoring the signal at the end of the transmission line as the probe was rotated about the x axis to vary the angle θ_i. Data were taken on both sides of the plane of symmetry for the probe ($\theta_i=\pi/2$) and averaged to produce a single pattern. The system was calibrated to be certain that the diode was operating in the square-law region over the range of measurement. The measured and theoretical field patterns are compared in Fig. 13(a), and they are seen to be in good agreement. Note that the position of the null in the pattern is shifted from $\theta_i=0°$, the point where it would occur for an ideal electrically short dipole with the pattern $|\sin\theta_i|$. This shift is about 5° which agrees well with the predictions of the theory (34).

In this example, the distortion of the field pattern by the resistive transmission line was minor. To test the theory further, a highly conducting transmission line was used

[3] The details of the equivalent circuit for the diode and its use in the equivalent circuit for the field probe are given in [10, ch. 3].

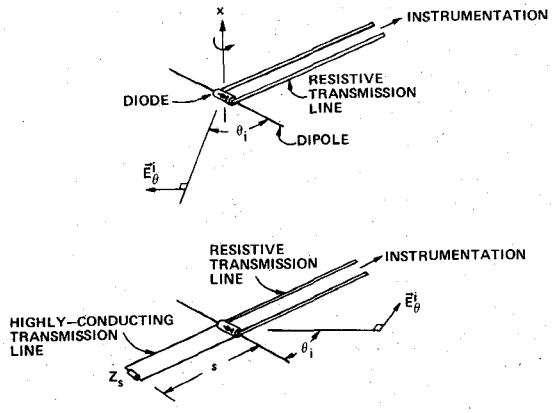

Fig. 12. Detail of experimental probe. (a) With resistive transmission line. (b) With highly conducting and resistive transmission lines.

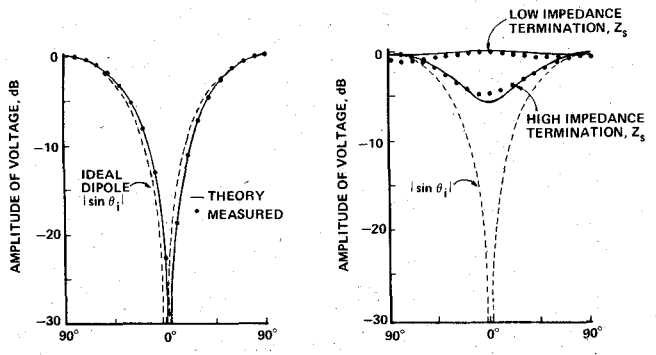

Fig. 13. Comparison of measured and theoretical field patterns in plane $\phi_i = \pi/2, 3\pi/2$ with incident field E_θ^i. (a) Resistive transmission line. (b) Highly conducting transmission line.

with the probe. The conductors of the line were copper with the dimensions $a_L = 0.32$ mm and $s = 7.0$ cm. At the high frequency used in this experiment, it is difficult to terminate the highly conducting parallel-wire transmission line in a known impedance and to precisely measure the voltage across that impedance without interfering with the reception of the incident signal by the dipole. To overcome this difficulty, the highly conducting transmission line was placed in parallel with the resistive transmission line already described, see Fig. 12(b). Since the resistive line was shown to have a minor effect on the field pattern of the probe, the pattern measured in this manner is approximately that of the dipole with the highly conducting transmission line.

Field patterns were measured with the highly conducting transmission line terminated in two different impedances Z_s: an open circuit and a low impedance formed by a lumped capacitor, $|Z_s/Z_c| \approx 0.17$. These patterns are compared with the theoretical results in Fig. 13(b), and they are seen to be in good agreement. Note that the theoretical results for the highly conducting transmission line were computed from the general expression (19), which is a function of the length of the line s and load impedance Z_s.

A comparison of Fig. 13(a) and (b) shows the great improvement in the field pattern of the probe obtained by replacing a highly conducting transmission line with a highly resistive one.

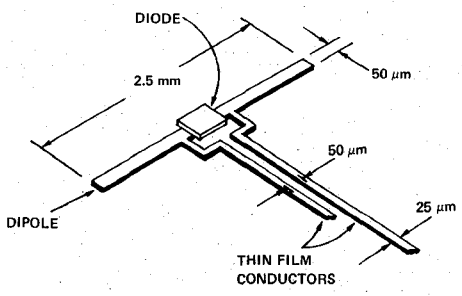

Fig. 14. Detail of the BRH probe.

VII. Summary and Conclusions

The electric field probe with the configuration shown in Fig. 1 has been analyzed to determine the effects of the lossy transmission line on its performance. The following conclusions can be drawn from the analysis.

i) The reception of the incident field by the transmission line distorts the field pattern of the probe from that of an ideal electrically short dipole antenna. For a highly resistive transmission line, the distortion of the pattern is proportional to the parameter χ (31); this includes the distortion that is the reception of a signal polarized so that it will not be received directly by the dipole. In the design of a field probe, this parameter is useful for comparing the distortion produced by different line geometries.

ii) The scattering of the incident field by the transmission line was shown to be greatly reduced by making the conductors highly resistive; hence the reason for referring to such lines as "transparent." The simple expressions developed for the total scattering cross section and the backscattering cross section of the highly resistive line (57)–(63) can be used to obtain a relative measure of the scattering from different line geometries and for comparing the scattering from the line with that from the dipole.

iii) The highly resistive transmission line behaves as a low-pass filter. If the probe is used to measure amplitude-modulated signals, the significant frequencies in the square of the modulating signal must be within the passband of this filter. For practical probes this will be true when the highest frequency f_m in the band-limited modulating signal satisfies the inequality $f_m \ll (8\pi c r^i s^2)^{-1}$.

To illustrate the use of these results, consider the miniature field probe in Fig. 14 recently developed by the U.S. Bureau of Radiological Health (BRH) for the measurement of amplitude-modulated fields with carrier frequencies in the range 0.2–12 GHz and modulating signals with frequency content in the range $0 \leqslant f \leqslant 2$ kHz [6]. The parameters for this probe were selected empirically. The dipole antenna is formed from a flat strip of half length $h = 1.25$ mm and width $w = 50$ μm; this strip is equivalent to a round conductor with a radius $a_A \approx w/4 = 13$ μm [16]. The conductors of the high-resistance transmission line are of length $s = 6.5$ cm and spacing $b = 50$ μm. The resistance per unit length of the thin-film conductors is $r^i \approx 9.7$ MΩ/m, and the capacitance per unit length of the transmission line is $c \approx 57$ pF/m. The transmission line is extremely lossy at the frequencies in the range of measurement; the exponential in (22) being $e^{-\alpha_L s} \leqslant e^{-54}$. The

parameter χ (31) is very small, $\chi = 7.1 \times 10^{-4}$; thus the distortion of the field pattern due to the transmission line is negligible. The theoretical shift in the nulls of the dipole pattern (34) is only $\Delta\theta \approx 0.04°$.

The normalized total scattering cross section for the transmission line $\sigma_L(0, \pi/2; 0)/\lambda_0^2$ is determined approximately by the small argument formula (62) at the lowest frequency 0.2 GHz ($\beta_0 s = 0.27$) and by the asymptotic value (63) at the highest frequency 12 GHz ($\beta_0 s = 16.3$). The ratio of the total scattering cross section per unit length of the transmission line to that for the dipole antenna $[\sigma_L(0, \pi/2; 0)/s]/[\sigma_A(\pi/2; 0)/2h]$ decreases from 10^4 at 0.2 GHz to 0.9 at 12 GHz.

The quantity $|k_L(\omega)s|^2$ (71) is equal to one at the frequency $f = 34$ kHz; thus a field can be measured with little distortion when the maximum frequency in the amplitude modulation is $f_m \ll 17$ kHz. This requirement is well satisfied when the probe is used within specifications, $f_m = 2$ kHz.

ACKNOWLEDGMENT

The author wishes to thank Dr. T. Batchman of the University of Virginia and H. Bassen of the Bureau of Radiological Health for their helpful comments on the work presented in this paper, and D. Marcovitch for assistance with the measurements.

REFERENCES

[1] C. L. Andrews, "Diffraction pattern in a circular aperture measured in the microwave region," *J. Appl. Phys.*, vol. 21, pp. 761–767, Aug. 1950.

[2] A. W. Rudge, "An electromagnetic radiation probe for near-field measurements at microwave frequencies," *J. Microwave Power*, vol. 5, pp. 155–174, Nov. 1970.

[3] F. Greene, "Development of electric and magnetic near field probes," Nat. Bur. Stand. Tech. Note 658, Jan. 1975.

[4] R. R. Bowman, "Some recent developments in the characterization and measurement of hazardous electromagnetic fields," in *Biological Effects and Health Hazards of Microwave Radiation*. Warsaw, Poland: Polish Medical Publishers, 1974, pp. 217–227.

[5] H. Bassen, M. Swicord, and J. Abita, "A miniature broad-band electric field probe," *Annals of the New York Academy of Sciences, Biological Effects of Nonionizing Radiation*, vol. 297, pp. 481–493, Feb. 1975.

[6] H. Bassen, W. Herman, and R. Hoss, "EM probe with fiber optic telemetry," *Microwave J.*, vol. 20, pp. 35–39, Apr. 1977.

[7] H. Bassen, P. Herchenroeder, A. Cheung, and S. Neuder, "Evaluation of an implantable electric-field probe within finite simulated tissues," *Radio Sci.*, vol. 12, pp. 15–25, Nov.–Dec. 1977.

[8] G. S. Smith, "A comparison of electrically short bare and insulated probes for measuring the local radio frequency electric field in biological systems," *IEEE Trans. Biomed. Eng.*, vol. BME-22, pp. 477–483, Nov. 1975.

[9] ——, "The electric-field probe near a material interface with application to the probing of fields in the biological bodies," *IEEE Trans. Microwave Theory Tech.*, vol. MTT-27, pp. 270–278, Mar. 1979.

[10] R. W. P. King and G. S. Smith, *Antennas in Matter: Fundamentals, Theory and Applications*. Cambridge, MA: M.I.T. Press, 1981, ch. 3.

[11] S. H. Mousavinezhad, K.-M. Chen, and D. P. Nyquist, "Response of insulated electric field probes in finite heterogeneous biological bodies," *IEEE Trans. Microwave Theory Tech.*, vol. MTT-26, pp. 599–607, Aug. 1978.

[12] C. D. Taylor, R. S. Saterwhite, and C. W. Harrison, Jr., "The response of a terminated two-wire transmission line excited by a nonuniform electromagnetic field," *IEEE Trans. Antennas Propagat.*, vol. AP-13, pp. 987–989, Nov. 1965.

[13] A. A. Smith, Jr., *Coupling of External Electromagnetic Fields to Transmission Lines*. New York: Wiley-Interscience, 1977.

[14] R. W. P. King and T. T. Wu, *The Scattering and Diffraction of Waves*. Cambridge, MA: Harvard Univ. Press, 1959.

[15] J. H. Van Vleck, F. Bloch, and M. Hamermesh, "Theory of radar reflection from wires or thin metallic strips," *J. Appl. Phys.*, vol. 18, pp. 274–294, Mar. 1947.

[16] R. W. P. King, *The Theory of Linear Antennas*. Cambridge, MA: Harvard Univ. Press, 1956.

[17] R. F. Harrington, *Field Computations by Moment Methods*. New York: Macmillan, 1968.

[18] F. G. Tricomi, *Integral Equations*. New York: Wiley-Interscience, 1957.

[19] M. Abramowitz and I. A. Stegun, *Handbook of Mathematical Functions*. Washington, DC: U.S. Gov. Printing Office, 1964.

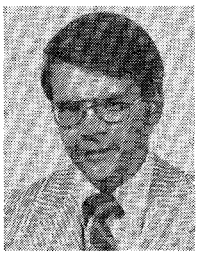

Glenn S. Smith (S'65–M'72–SM'80) was born in Salem, MA, on June 1, 1945. He received the B.S.E.E. degree from Tufts University, Medford, MA., in 1967 and the S.M. and Ph.D. degrees in applied physics from Harvard University, Cambridge, MA, in 1968 and 1972, respectively.

From 1969 to 1972 he was Teaching Fellow and Research Assistant in Applied Physics at Harvard University. From 1972 to 1975 he served as a Postdoctoral Research Fellow at Harvard University and also as a part-time Research Associate and Instructor at Northeastern University, Boston, MA. He is presently an Associate Professor of Electrical Engineering at Georgia Institute of Technology, Atlanta, GA.

Dr. Smith is a member of Tau Beta Pi, Eta Kappa Nu, and Sigma Xi.